Super-selective reconstruction of causal and direct connectivity with application to *in-vitro* iPSC neuronal networks

Francesca Puppo[a,*], Deborah Pré[b,*], Anne Bang[b,**], Gabriel A. Silva[c,**]

[a] *BioCircuits Institute, Center for Engineered Natural Intelligence, University of California, San Diego, La Jolla, 92093 CA, USA*
[b] *Conrad Prebys Center for Chemical Genomics, Sanford Burnham Prebys Medical Discovery Institute, La Jolla, CA 92037, USA*
[c] *Department of Bioengineering, Department of Neurosciences, BioCircuits Institute, Center for Engineered Natural Intelligence, University of California, San Diego, La Jolla, 92093 CA, USA*

Abstract

Despite advancements in the development of cell-based *in-vitro* neuronal network models, the lack of appropriate computational tools limits their analyses. Methods aimed at deciphering the effective connections between neurons from extracellular spike recordings would increase utility of *in-vitro* local neural circuits, especially for studies of human neural development and disease based on induced pluripotent stem cells (hiPSC). Current techniques allow statistical inference of functional couplings in the network but are fundamentally unable to correctly identify indirect and apparent connections between neurons, generating redundant maps with limited ability to model the causal dynamics of the network. In this paper, we describe a novel mathematically rigorous, model-free method to map effective - direct and causal - connectivity of neuronal networks from multi-electrode array data. The inference algorithm uses a combination of statistical and deterministic indicators which, first, enables identification of all existing functional links in the network and then, reconstructs the directed and causal connection diagram via a super-selective rule enabling highly accurate classification of direct, indirect and apparent links. Our method can be generally applied to the functional characterization of any *in-vitro* neuronal networks. Here, we show that, given its accuracy, it can offer important insights into the functional development of *in-vitro* iPSC-derived neuronal cultures by reconstructing their effective connectivity, thus facilitating future efforts to generate predictive models for neurological disorders, drug testing and neuronal network modeling.

Keywords: neural network, effective connectivity, functional connectivity, causality, apparent connectivity, correlation, MEA, iPSC, development

1. Introduction

In-vitro cultures of primary neurons can self-organize into networks that generate spontaneous patterns of activity [1, 2, 3], in some cases resembling aspects of developing brain circuits [4, 5]. The emergent functional states exhibited by these neuronal ensembles have been the focus of attention for many years [6, 7] as they can be used to investigate principles that govern their development

*These two authors contributed equally
**Corresponding authors
Email addresses: email: abang@SBPdiscovery.org (Anne Bang), email: gsilva@ucsd.edu (Gabriel A. Silva)

and maintenance [8, 9] and to produce biological correlates for neural network modeling [10, 11]. In humans, in the absence of intracranial recording electrodes, neither physiological nor pathological network activity can be studied *in vivo*. The introduction of human induced-pluripotent stem cell (hiPSC) technologies [12, 13] opened the possibility to generate *in-vitro* neuronal networks in typical [14, 15], as well as patient-specific genetic backgrounds [16, 17, 18, 19, 20, 21], demonstrating the potential to reproduce key molecular and pathophysiological processes in highly controlled, reduced, experimental models that enables the study of neurological disorders and the discovery and testing of drugs, especially in the context of the individual patient [22, 23, 24].

One common approach to obtain information from *in vitro* neuronal networks is to record their activity via multi-electrode array (MEA) or calcium fluorescence imaging and then use network activity features to describe their physiology. One main limitation, however, is that these high-dimensional data, which report about the information representation in the network, do not translate into a clear understanding of how this representation was produced and how it emerged based on neuronal connectivity [25]. The synchronization of spontaneous spike trains among different MEA sites or neurons, also referred to as network bursting, is an example of observed neural behaviors widely reported in the literature. The generation of network bursting in an *in vitro* neuronal culture is evidence that the neurons are synaptically connected. However, the extracellular nature of the MEA recording does not provide information about how neurons are connected and how signals propagate between them, such that computational analyses are necessary to reconstruct their complex dynamic patterns.

Knowing how neurons are connected and how they exchange information in complex, dynamic patterns can be useful for investigating neural mechanisms as it allows for identification of functional states and directly relates their emergence to the underlying wiring diagram [11]. This kind of analysis presents several challenges as it requires not only identification of functional relationships between cells, but also reconstruction of the dynamic causality between directly linked neurons that are simultaneously involved in several different signaling pathways. This is the difference between functional and effective inference: the first only reports about statistical dependencies between cells' activities without giving any information about specific causal effects existing between two neurons or the underlying structural model [26]; the second attempts to capture a network of effective - direct and causal - effects between neural elements [27].

Only model-based approaches [25, 28] have been proposed for inference of effective connectivity. Among them, dynamic causal modeling (DCM) [29] and structural equation modeling [30] variants have shown best performances (Figure 1). However, these methods estimate the effective connectivity of a measured neuronal network by explicitly modeling the data generation process, i.e. only the connectivity of a simulated network model is inferred without any theoretical guarantee about its accuracy and its ability to correctly estimate the connectivity of the biological network [25, 26].

Because of this limitation, descriptive, model-free approaches are usually preferred as they are easy to implement, rely on a limited number of assumptions that are directly related to the investigated neuronal network, and can be easily tested [25, 28]. A number of model-free methods proposed for reconstructing the connectivity of *in vitro* neuronal networks [31] have been previously reviewed [32] and tested [26] (Figure 1). However, because they rely on purely statistical indicators, they can only infer how neurons are functionally coupled, but lack the ability to identify the network of effective interactions between neurons by either missing the directionality or confounding indirect and apparent links from direct ones. Directionality conveys the causality of signaling in the network, i.e. which neural element has causal influences over another; indirect connectivity indicates

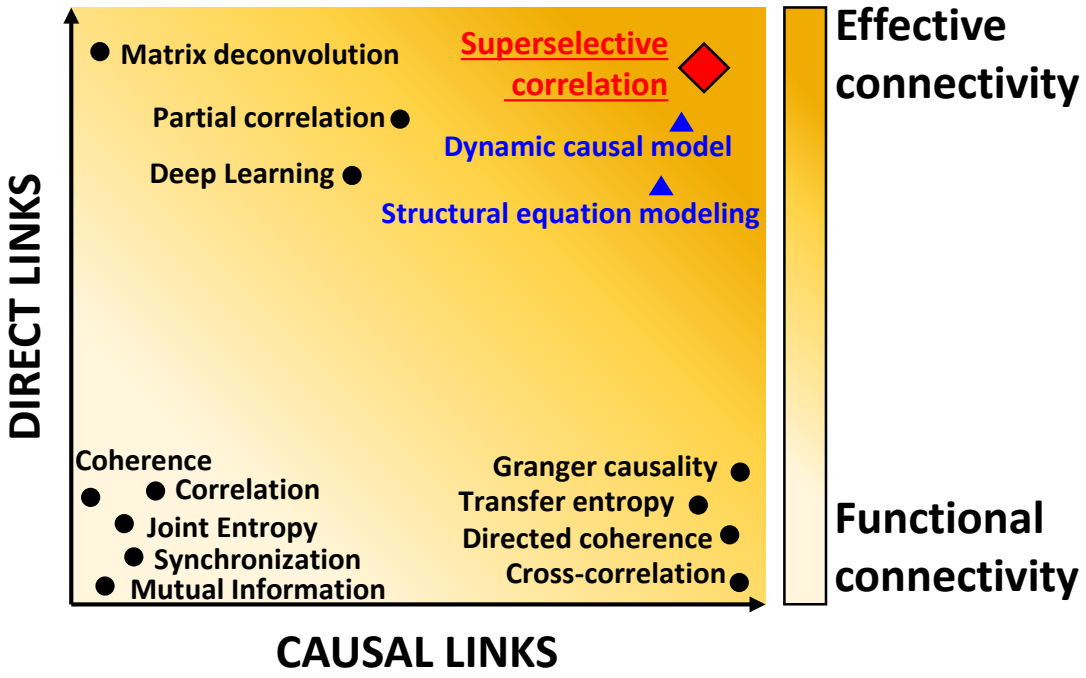

Figure 1: **Classification of most common connectivity inference methods in terms of causality and detection of direct links**. On the x-axes, the graph shows a scale of causality which refers to the ability of a given connectivity method to infer or not the directionality of the functional connections between neurons. On the y-axes, it visually quantifies the capabilities of one approach to detect direct links between neurons by identifying and discarding multi-neurons connections and apparent ones. Indicators that are acausal and do not infer directed links can only report about functional connectivity (light yellow); indicators which contain information about direction of interaction and direct neuron-to-neuron communication are also close to the inference of effective connectivity (orange color). Most common model-free techniques are indicated with black dots. Model-based methods are reported with blue triangles and their ability to infer effective connectivity is negatively weighted by the impossibility to test their performances. The super-selective correlation approach we propose is reported in red. The graph is meant for visual quantification and do not contain precise quantitative information about differences between methods.

the presence of multi-neurons pathways between two cells; apparent connectivity refers to the ability to disambiguate the confounding effects of common inputs from other participating neurons, that are manifest as functional connectivity, from those induced by neuronal connections between two units [33].
Methods such as correlation [34], coherence [35, 36, 37], mutual information [31, 38, 39], phase and generalized synchronization [39, 40], and joint entropy [31] describe only statistical dependencies between recorded neurons without carrying any information of causality or discriminating direct and indirect effects. Techniques such as cross-correlation [31, 41], directed and partial directed coherence [42, 43], transfer entropy [31, 41, 44] and Granger causality [45, 46] are examples of causal indicators as they provide inference of directionality of dependence between time series based on time or phase shifts, or prediction measures. However, because these operators rely only on pairwise statistical comparisons and treats pairs of neurons independently, they show the same limitations when dealing with indirect connections and external inputs. Only a few techniques can compete in the challenge of inferring the effective connectivity of a network. Partial-correlation [31, 47], which takes into account all neurons in the network, showed best performance in detecting direct associations between neurons and filtering out spurious ones [48]. The most significant limitation of this solution is its high computational cost. Moreover, as the partial correlation matrix is symmetric, this method is not useful for detecting the causal direction of neuronal links. It also does not attempt to infer self-connections [25]. A combination of correlation and network deconvolution was used by Magrans and Nowe [49] to infer a network of undirected connections with elimination of arbitrary path lengths caused by indirect effects. However, this method also can not identify directions of connections and the singular value decomposition of network deconvolution has an extremely high computational complexity [48]. A convolutional neural network approach [50] showed the same limitations in computational complexity and undetected self- and causal connections. Figure 1 graphically summarizes the inference capabilities of the state-of-the-art connectivity methods.

Here, we propose a novel, mathematically rigorous method that uses a model-free approach (i.e. does not depend on a set of underlying assumptions about the biology of participating cells) to decompose the complex neural activity of a network into a set of numerically validated direct, causal dependencies between the active component neurons that make up the network. The method is not purely statistical, like those previously proposed (Figure 1). Our algorithm combines the inference power of statistical approaches (signal-, network- and information theory- based) with the rigorousness of deterministic measures (a mathematical super-selection rule on top of the statistics) to derive causal rather than functional links through association of cause and effect and distinction between indirect and apparent links from actual one-to-one neural interactions. The analysis results in a fine-tuned selection of correlation peaks which maps to a subset of direct causal dependencies that more realistically describe the effective connectivity of the network (Figure 2).

To evaluate the performances of our method, we built a numerical model by designing and simulating an integrate-and-fire neuronal network mimicking the activity of *in vitro* cultures of neurons, and demonstrated important improvements, relative to the state-of-the-art connectivity methods, to network inference accuracy due to a deterministic component of our method capable of identifying false positive connections.

Importantly, our connectivity algorithm yields a computational complexity that scales as $O(n^2)$. This complexity is typical of connectivity methods based on pairwise statistical studies which, contrary to our method, are unable to detect false positive connections. In reconstructing the direct connectivity of a network, the technique we propose competes with partial correlation, but this latter

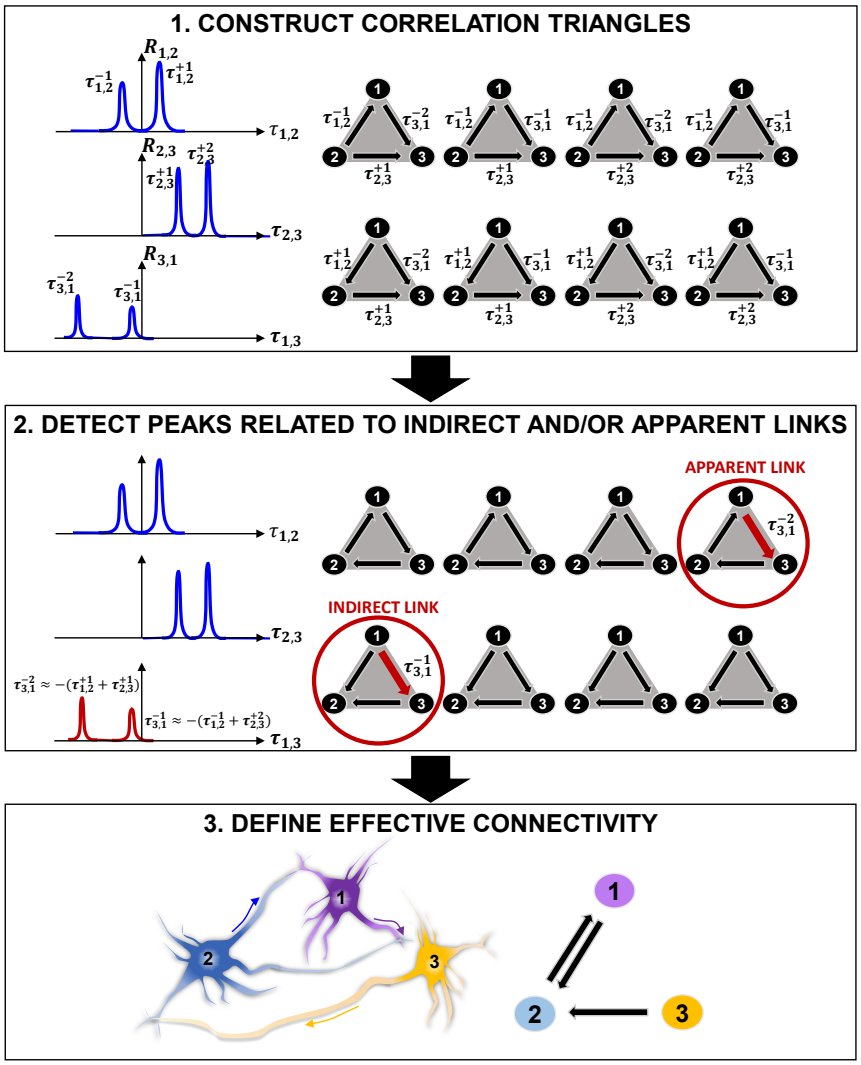

Figure 2: **Connectivity reconstruction via detection of correlation triangles and classification of indirect and apparent links**. 1. Given three neurons 1, 2 and 3, our algorithm searches, in time, for all correlations between them by computing the pairwise correlation functions $R_{1,2}$, $R_{2,3}$ and $R_{3,1}$. In this representative example, the algorithm detects two correlation peaks for each pair of neurons and associates the corresponding delays of interactions ($\tau_{1,2}^{-1}$, $\tau_{1,2}^{+1}$, $\tau_{2,3}^{-1}$, $\tau_{2,3}^{-2}$, $\tau_{3,1}^{+1}$, $\tau_{3,1}^{+2}$) which are defined by the location of the peaks with respect to the origin of the x axis. 8 possible combinations of interactions can occur in time between the three pairs of neurons. These correspond to the 8 correlation triangles shown on the right side of the panel. 2. Among the correlation triangles, the algorithm detects 2 critical cases ($|\tau_{1,2}^{-1} + \tau_{2,3}^{-2} + \tau_{3,1}^{+1} < \epsilon|$ and $|\tau_{1,2}^{+1} + \tau_{2,3}^{-1} + \tau_{3,1}^{+2} < \epsilon|$) and identifies the peaks relative to an indirect (multi-neurons path) and an apparent (common output) connection by searching for the ones with smaller amplitude. The smallest peaks ($\tau_{3,1}^{+1}$ and $\tau_{3,1}^{+2}$) are discarded from the analysis. 3. The correlation triangles are functional to the estimation of the direct connections in the network. Because no more correlation exists between neuron **1** and **3**, the estimated effective connectivity includes only the direct links for $(1, 2)$ and $(3, 1)$: two connections with opposite directionality exist between neuron 1 and 2 because positive and negative correlation peaks are detected in $R_{1,2}$ ($\tau_{1,2}^{-1}$ and $\tau_{1,2}^{+1}$); one link connects neuron 2 to neuron 3 as a result of the positive correlation peaks in $R_{2,3}$ ($\tau_{3,1}^{+1}$ and $\tau_{3,1}^{+2}$).

yields a complexity of $O(n^3)$.

We show an experimental application of our approach to spontaneously generated *in vitro* networks of human iPSC-derived neurons cultured on MEAs providing an analysis and interpretation of the physiology not possible otherwise. We describe the temporal evolution associated with the connectivity and dynamic signaling of developing hiPSC-derived neuronal networks, including increasing synchronized activity and the formation of small numbers of hyper-connected hub-like nodes, as similarly reported by others [14, 20]. These results further support the performance quality of our approach and provide an example of how this connectivity method can be used to characterize network formation and dynamics, thus facilitating efforts to generate predictive models for neurological disease, drug discovery and neural network modeling.

2. Theoretical framework for connectivity reconstruction

2.1. Algorithm outline

The proposed analysis takes, as inputs, electrophysiological recordings from hiPSC-derived neurons on MEAs and decomposes the collective firing properties into direct (one-to-one) and causal (directional) relationships between all participating neurons by means of a multi-phase approach that identifies and discards any correlation link that does not directly relate to a direct interaction between two cells.

The core of our methodology is graphically described in Figure 2 and includes three main phases: 1. statistical, correlation-based reconstruction of functional connectivity (Section 2.2; 2. mathematically-rigorous super-selection of direct links via identification of peaks related to indirect and apparent links (Section 2.3) and 3. reconstruction of directed causal connectivity between neurons (Section 2.4).

1. The functional connectivity (statistical dependencies) of a network is computed via pairwise correlation studies. Functional interactions between neurons are represented by correlation peaks and their delays $\boldsymbol{\tau}$ (see Section 2.2.1). The algorithm constructs ***correlation triangles*** by considering all possible combinations of correlation delays for any possible triplet of neurons (Figure 2.1). Importantly, correlation triangles do not refer to any three-neuron physical connection, sometimes referred to as "neural triangles" in the literature and known to be highly represented among possible neural interaction patterns [51, 52]. Here we define a correlation triangle as a mathematical object that our algorithm uses to classify functional interactions based on all possible triplets of correlation delays that can be formed in the network. Therefore, correlation triangles exploit the entire signal history of neurons in order to determine the correlation peaks.
2. Correlation peaks associated with indirect or apparent links in corresponding correlation triangles are discarded from the analysis by means of a mathematical super-selection rule which deterministically classifies the type of dependence between each triplets of neurons (Figure 2.2). The super-selection rule is formally presented in Section 2.3. Here, it can be summarized as follow. If a correlation triangle is made up of three correlation delays that are the combination of one another (see Section 2.3.1), one of the component correlation delays is either representative of an indirect link (two neurons connected but only through an intermediary cell) or of an apparent link (functional coupling due to synchronous activity of two neurons on the same output neuron); therefore, this correlation delay does not refer to an effective connection and must be discarded. When the algorithm finds a correlation triangle which satisfies this condition, it deepens into the classification of the involved correlation delays and select

the correlation peak to remove based on the peaks amplitude (see Section 2.3.2 for a detailed explanation). For example, in Figure 2.2, the algorithm identifies an indirect link between 1 and 3 (a multi-neuron pathway), and an apparent link between 1 and 3 (correlation due to a common output). The correlation peaks corresponding to these links in the correlation triangles are discarded from the analysis. Importantly, the algorithm removes correlations from the analysis, but does remove inferred physical connections.

3. Only when all correlation peaks between two neurons are discarded, the algorithm recognizes that a specific interaction is only apparent and deletes the corresponding connection. For example, in Figure 2.3, there is no existing connection between neurons 1 and 3. The estimated effective connectivity includes only direct links for $(1, 2)$ and $(2, 3)$: two connections with opposite directionality exist between neuron 1 and 2 because positive and negative correlation peaks are detected in $R_{1,2}$ ($\tau_{1,2}^{-1}$ and $\tau_{1,2}^{+1}$); one link connects neuron 2 to neuron 3 as a result of the positive correlation peaks in $R_{2,3}$ ($\tau_{2,3}^{+1}$ and $\tau_{2,3}^{+2}$). Section 2.4 formally presents the reconstruction rule of our algorithm.

The following sections describe the mathematical details of the developed technique. The connectivity reconstruction algorithm and associated functions for performance evaluation were implemented in Matlab and code will be made available online.

2.2. Reconstruction of functional connectivity

2.2.1. Temporal correlations

To identify the temporal correlations between the activity of all pairs of N recorded neurons $j, k \in \{1, ..., N\}$ in the network, we computed the pairwise correlation function between the corresponding signals s_j and s_k

$$R_{jk}(\tau) = \int s_j(t)s_k(t + \tau)dt \tag{1}$$

In this formulation, the indexes j and k are restricted to $k > j$ in order to avoid unnecessary calculation of auto-correlations ($j = k$) and explicitly calculate correlations only for $k > j$ because, thanks to the symmetry of (1),

$$R_{jk}(\tau) = R_{kj}(-\tau). \tag{2}$$

Using the Fast Fourier Transform (FFT) and the correlation theorem, computing correlations in Eq. (1) can be efficiently performed in $O(n \log n)$ with n the number of samples composing the signals s_j. In fact, if $\mathcal{F}$ is the FFT operator and $\mathcal{F}^{-1}$ the corresponding inverse, the correlations can be efficiently computed as $R_{jk}(\tau) = \mathcal{F}^{-1}[\mathcal{F}[s_j] \cdot \mathcal{F}[s_k]]$ [53].

Peaks of $R_{jk}(\tau)$ represent correlations among neurons j and k. Their amplitude can be regarded as a measure of the level of correlation between the spikes in their registered firing activities. The higher the amplitude of a peak in $R_{jk}(\tau)$ (if any), the higher the probability that there is a statistical dependency between neuron j and neuron k. However, the existence of a functional coupling between two neurons does not necessarily imply that there is an effective connection between them. For example, the activity of any of the two neurons can have an effect on the other through one or more interconnecting cells between them.

The location of each correlation peak with respect to the origin indicates the temporal delay τ_{jk}^{peak} between the activity of neuron j and neuron k. The sign of this delay, i.e. whether the peak is found on the positive or the negative quadrant of the correlation function, defines the directionality of the interaction that, in the ideal case of a direct connection, suggests which is the pre- and post-synaptic neuron in the interaction.

2.2.2. Peak detection

We implemented a peak detection algorithm applied to $R_{jk}(\tau)$ to identify all existing functional correlations between any pair of neurons (j,k) in the network and to discern the directional dependency between their spiking activities (Figure S.2).

As part of the peak detection phase, we used a smoothing Gaussian filtering [54] applied directly to $R_{jk}(\tau)$ to remove high frequencies and facilitate the proper identification of correlation peaks.

As introduced above, we assume that a correlation peak in $R_{jk}(\tau)$ represents a potential connection between j and k and that τ_{jk}^{peak} is the signal propagation delay between them. We define a temporal range $(-T,+T)$ over which to perform the peak search (Section 2.4 describes the details of parameter tuning).

For a given parameterization of the Gaussian filter (see Section 2.4) and a defined time window $(-T,+T)$, the peak detection algorithm allows us to identify a list of pairwise temporal delays τ_{jk}^{h} between all pairs of neurons (j,k) in the observed network, with $h \in \{-h_n,...,-1,1,...,h_p\}_{jk}$ where h_n is the number of peaks with $\tau_{jk}^{h} < 0$ and h_p the number of peaks with $\tau_{jk}^{h} > 0$. Peaks identified on the positive ($\{1,...,h_p\}_{jk}$) or negative ($\{-h_n,...,-1\}_{jk}$) side indicate whether the spiking activity of neuron j has temporally occurred, respectively, before ($\tau_{jk}^{h} > 0$) or after ($\tau_{jk}^{h} < 0$) the firing of neuron k. Finally, from Eq. (2) the following relation holds:

$$\tau_{jk}^{h} = -\tau_{kj}^{-h}. \tag{3}$$

2.3. Detection of false positive connections

Correlation peaks detected in $R_{jk}(\tau)$ represent any type of statistical dependence between two neurons. Peaks relative to functional dependencies due to multi-neuron connections or apparent coupling are the main cause of false positives generated in the connectivity reconstruction process and a major source of error in competing methods. To address this, we introduce a framework that identifies the effective network configuration via implementation of a deterministic super-selection rule over all the detected correlation triangles.

2.3.1. Pure direct connections and correlation triangles

In order to identify possible dependencies between correlations, i.e., if a correlation among neurons is not direct but results from a third party correlation, we consider *cyclic* triplets of correlation delays $(\tau_{jk}^{h}, \tau_{km}^{h'}, \tau_{mj}^{h''})$. Here cyclic means that each neuron's index appears in two ordered neuron's index pairs, once as the first index and once as the second index. This cyclicity directly implies that, if we had

$$\tau_{jk}^{h} + \tau_{km}^{h'} + \tau_{mj}^{h''} = 0, \tag{4}$$

one of the three delays would result from signals that correlate through an intermediary signal as shown in Fig. 2.

However, since the correlations among the neurons' firing are not Dirac deltas but rather Gaussian-like, we can define a threshold $\epsilon > 0$ such that a weak version of (4) still holds. Therefore Eq. (4) reads

$$|\tau_{jk}^{h} + \tau_{km}^{h'} + \tau_{mj}^{h''}| < \epsilon \tag{5}$$

This equation identifies the case where there is a near-perfect match between the correlation delay of each of the three cells and represents the first step in the proposed super-selection algorithm. The definition of "near-perfect match" is based on the choice for the parameter ϵ which represents the acceptable degree of temporal approximation when computing Eq. 5 (see Section 2.4 for an estimation and a discussion on ϵ). In ideal conditions, $\epsilon \to 0$ and Eq.(5) reduces to Eq.(4).

Finally, it is useful to define a correlation triangle as the triplet $(\tau^h_{jk}, \tau^{h'}_{km}, \tau^{h''}_{mj})$ of cyclic correlation delays that the algorithm detects for any pair of neurons in the network. The algorithm aims to construct $n_{jk} \times n_{km} \times n_{mj}$ correlations triangles given by all possible combinations of correlation peaks of any triplet of neurons' pairs (Figure 2). To have a complete picture of our method, we can define the directed graph $G = (V, E)$ whose vertexes V are the active neurons and edges E are the active synaptic connections. This definition implies that our algorithm reconstructs only the connections between the neurons in the culture whose activity has been recorded, and contains no reference to the full structural connectivity of the biological network under study. Within this framework, each correlation triangle shares up to three edges with G, and the union E' of all τ^h_{jk} defines the direct graph $G' = (V, E')$. It follows that

$$G \subseteq G'. \tag{6}$$

G' can overestimates G because it could include connections that are false positives (Figure 2A). For this reason, we need to determine an efficient minimization scheme to reduce G' as close as possible to G.

2.3.2. Edge covering minimization

In order to reduce G' to G it is sufficient that for each correlation triangle satisfying Eq. (4) (or Eq. (5)) we identify the dependent τ^h_{jk} and remove it from E'. Therefore, the challenge is to find a discrimination rule that allows us to select the correct τ^h_{jk} in the correlation triangles that satisfy Eq. (4) (or Eq. (5)).

By considering the nature of neuronal signals, we can define the discrimination factor based on the amplitude A^h_{jm} of correlation peaks. In fact, a neuron is equivalent to an input-output object that generates an output signal $s_{out}(t)$ either independently or dependently on an input signal $s_{in}(t)$ coming from another neuron. If s_{out} depends on s_{in}, the two signals are not perfectly synchronized but are often noisy (have a phase noise) resulting from the intrinsic excitability properties of the neurons. For example, when an incoming spike train from an input neuron activates an output neuron, the timing of the output spiking depends on many biochemical factors including for example the state of voltage gated ion channels. The result is that the signal of the output neuron is never triggered at the same exact delayed time, but varies. The larger the variation of the delayed timing between the input and the output neurons, the larger the phase noise in the associated correlation peak which will have smaller amplitude and larger standard deviation than the correlation among neurons with input and output signals without phase noise and perfectly synchronized. Moreover, if the signals belong to two neurons that are interconnected via an intermediary cell, the phase noise is amplified and the correlation peak is even shorter (low amplitude) and wider (large standard deviation).

Therefore, within this picture, we can establish the second step in the super-selection algorithm as:

Given a correlation triangle $(\tau^h_{jk}, \tau^{h'}_{km}, \tau^{h''}_{mj})$, the delay associated with the smallest correlation peak amplitude

$$min(A^h_{jk}, A^{h'}_{km}, A^{h''}_{mj}) \tag{7}$$

estimates the false positive connection and is discarded from E'.

In the ideal case, i.e. without errors and approximations, this super-selection scheme eliminates all indirect correlations, and therefore reduces G' exactly to G.

Figure 3A reports a real case scenario of apparent connection. Three neurons (indexed 1, 4 and 12 in our model) from a recorded biological neuronal network are temporally related according to the visualized correlation triangle schema. The algorithm checks all correlation triangles in the recorded network and detects that this particular case satisfies Eq. 5 for a selected ϵ =3 ms. As explained in the following section, ϵ was taken equal to the mean width of the correlation peaks. One correlation delay matches the combination of the other two. The algorithm identifies which of the three peaks corresponds to an indirect or apparent link by comparing the peaks' amplitude. In the example, the delay $\tau_{1,4}$ corresponds to the smallest correlation peak and is therefore discarded from the analysis, i.e., from E'. If in the chosen temporal window that defines E' only $\tau_{1,4}$ is detected for neuron 1 and 4, the final reconstruction will not include any effective connection between 1 and 4. This is a nice example of marrying-parents effect [25] where an apparent link between neuron 1 and 4 is formed as a result of neuron 12 firing at the same time on both of them.

2.4. Connectivity matrix reconstruction

There are three fundamental parameters that affect the inference performance of this method:

- T defines the time window $(-T, +T)$ over which to search for correlation peaks in the correlation function R_{jk}. This parameter affects the filtering power of the connectivity algorithm. An optimal T depends on the specific activity properties of the neuronal network under analysis. To account for all direct neural interactions, the best time window should include the mean maximum propagation delay between the neurons in the network. If the window is too small, the algorithm can over-filter otherwise important correlation interactions.

- σ is the standard deviation (width) of the smoothing Gaussian filter and defines the frequencies to filter out in the correlation functions. σ is important because the location of the detected correlation peaks weakly depends on it. In fact, while the Gaussian filter is necessary for a more reliable peak detection, the level of smoothing introduces a small temporal jitter between the actual location of the peak and its filtered version.

- ϵ is the degree of uncertainty; it defines the threshold beyond which the correlation delays in a correlation triangle can be considered the combination of one another, i.e. how similar the combination of two correlation delays τ_{km} and τ_{mj} must be from the direct correlation delay τ_{jk} to estimate a three-neuron effective connectivity (see Eq. 5). Large ϵ values increase the number of detected correlation peaks and computed correlation triangles with the potential shortcoming that true positive connections are filtered out. Too small ϵ values are responsible for a poor filtering of spurious delays. A good approximation for ϵ is the mean width of the detected correlation peaks which represents the variance of the correlation delays. For example, if we consider the correlation peaks from the real case scenario in Figure 3, the width of the peaks is about 2.5 ms; therefore, we chose $\epsilon = 3$ ms as threshold value for our super-selection of direct links.

All three parameters should be tuned in order to have the best outcome from our method. The connectivity reconstruction approach we propose here is based on a parameter variation scheme that leads directly to the reconstruction of the effective connectivity matrix of the network.

Figure 4A-C reports about the performances of the algorithm for varying T, σ and a fixed ϵ equal to the mean of the width of the peaks. The performances were assessed based on the indicators TP/N_c (net number of true positive (TP) connections; N_c number of connections in the simulated

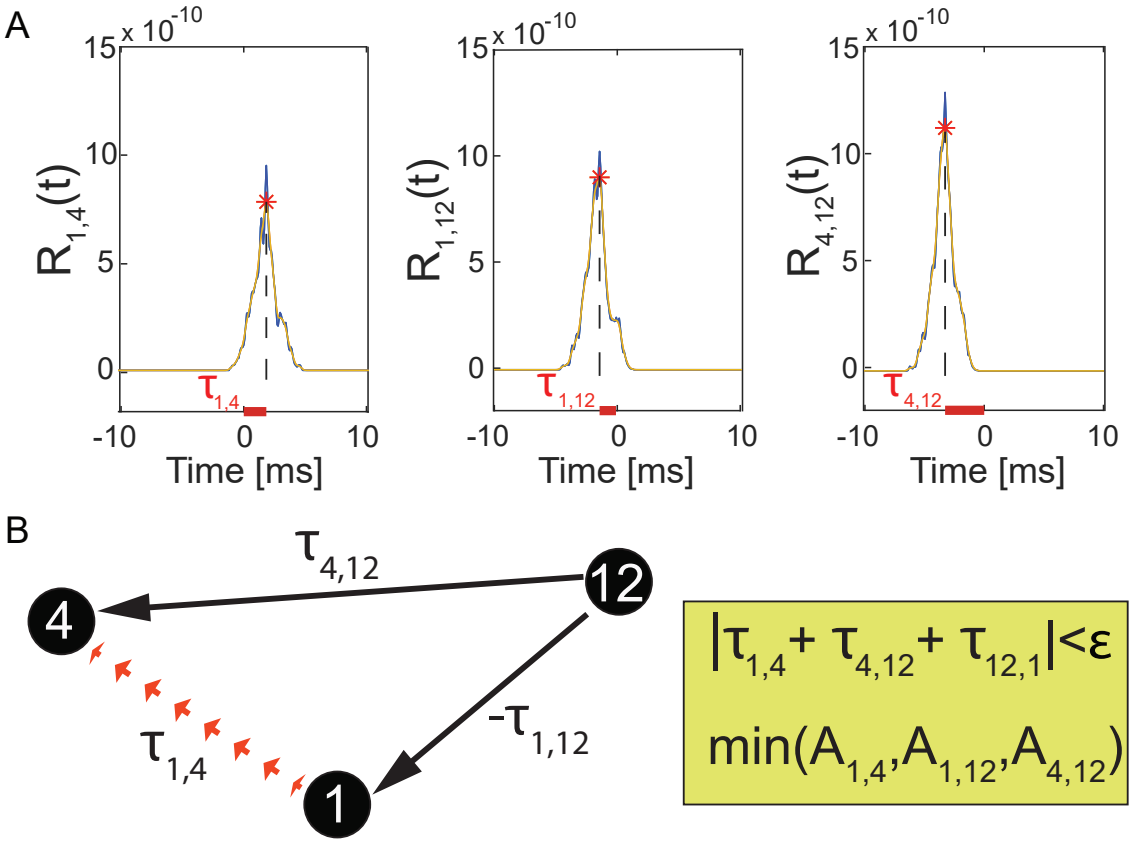

Figure 3: **Real case scenario of correlation triangles and detection of false positive connections**. (A) Correlation functions $R_{1,4}$, $R_{1,12}$, $R_{4,12}$ computed for pairs of biological neurons $(1,4)$, $(1,12)$, $(4,12)$ (blue line). The selected time window was (-20 ms, +20 ms), but the graph only shows a zoomed view in (-10 ms, +10 ms) to better describe the selection rule if only one correlation was detected in time between the neurons. The σ of the Gaussian filter was 0.0005 s, resulting in smoothed correlation signals (orange dashed line). The detected correlation peaks (red stars) represent functional correlations between neurons and their combinations define the correlation triangles that our algorithm uses to detect false positive connections. The horizontal offset between the position of each peak and the origin represents the temporal delay $\tau_{j,k}$ associated with these links. (C) These delays satisfy the cyclic condition on τ, i.e., $|\tau_{1,4}+\tau_{4,12}+\tau_{12,1}| = |\tau_{1,4}+\tau_{4,12}-\tau_{1,12}| < 3$ ms therefore indicating that one of the three correlations in the correlation triangle corresponds to an apparent link. The algorithm detects which of the three by searching for the correlation peak with smallest amplitude. In the example, $A_{1,4}$ has the smallest amplitude and the algorithm discards it from the analysis preventing generation of a false positive link.

neuronal network), FP/N_c (net number of false positive (FP) connections) and $\Delta = (TP - FP)/N_c$ (confidence indicator), as described in Section 3.1. This allowed us to individuate a range of values for T and σ where the inference performances of the connectivity method had reached a maximum plateau (Fig. 4D), and define the reconstruction rule of our algorithm as follows.
We consider a fixed value for ϵ. We then consider a collection of p points in the T-σ space (for example the nine points in Fig. 4D,E). The boundaries for σ and T can be chosen according to their definitions. For example, a minimum value for σ should be related to the very high frequency in the signal while the maximum value to the frequencies in the lower middle spectrum. A minimum value of T should be at least as large as 2-3 times the average delay among neurons to guarantee that the relevant peak are included in the analysis. On the other hand, the maximum value for T can be chosen as several times (for example 5-6) the average delay among neurons in order to include more correlation triangles later used to refine the selection.

For each point $p = (T, \sigma)$ we compute E'_p and perform the super-selection to minimize E'_p. Then, we compute the connectivity matrix M_p (e.g. Fig. 4F - see Section 3.1 for full details) with 1 in the (j, k) entry if the reduced E'_p contains at least one $\tau^h_{jk} > 0$, and 0 otherwise. We consider only $\tau^h_{jk} > 0$ because, according to Eq. (3), if $\tau^h_{jk} < 0$, E'_p includes $\tau^{-h}_{kj} > 0$ that corresponds to the same correlations.

We can therefore define the frequency for each connection in the connectivity matrix as

$$f_{jk} = \frac{1}{K} \sum_p M_{p_{jk}} \tag{8}$$

where K is the total number of computed points p. Each frequency computed in this way is a binary classifier for a given effective connection between neurons j and k. Therefore, introducing a discrimination threshold $0 \leq d \leq 1$, for each connection we can decide if it is true or false and compute true and false positive and true and false negative rates.

3. Experimental methodology

3.1. Numerical experiments

To develop and validate our connectivity method we used spiking data generated via simulations of neuronal networks based on the Izhikevich model [55]. The original code was modified to guarantee high levels of activity in the network as well as bursting like behavior similar to that registered in our experiments (see Appendix A.). Figure S.1 shows an example of a random network generated via the implemented model. We performed our analysis on sparse networks ($N_c << N_{tot}$, with N_c the number of connections in the simulated network and N_{tot} the total number of possible connections that can be formed given the input size of the investigated network model) that could be more easily simulated and analyzed with standard computational resources and that accurately described the sparse activity of the iPSC-derived neuronal networks we investigated. However, it is worth noting that our model is general and not restricted to sparse connectivity.

Standard metrics for assessing the inference properties of connectivity methods are the true positive rate, or sensitivity, $TPR = TP/N_c$ (TP is the number of true positives; N_c is the number of real positive connections in the data), the false positive rate, or specificity, $FPR = FP/(FP + TN)$ (FP is the number of false positives; TN is the number of true negative connections), and the Accuracy $ACC = (TP + FP)/N_{tot}$ ($N_{tot} = TP + TN + FP + FN$ is the total number of possible connections that can be formed given the input size of the simulated network) [56, 31]. However, in order to have a quantitative measure of the level of confidence in the detection of TPs, we also

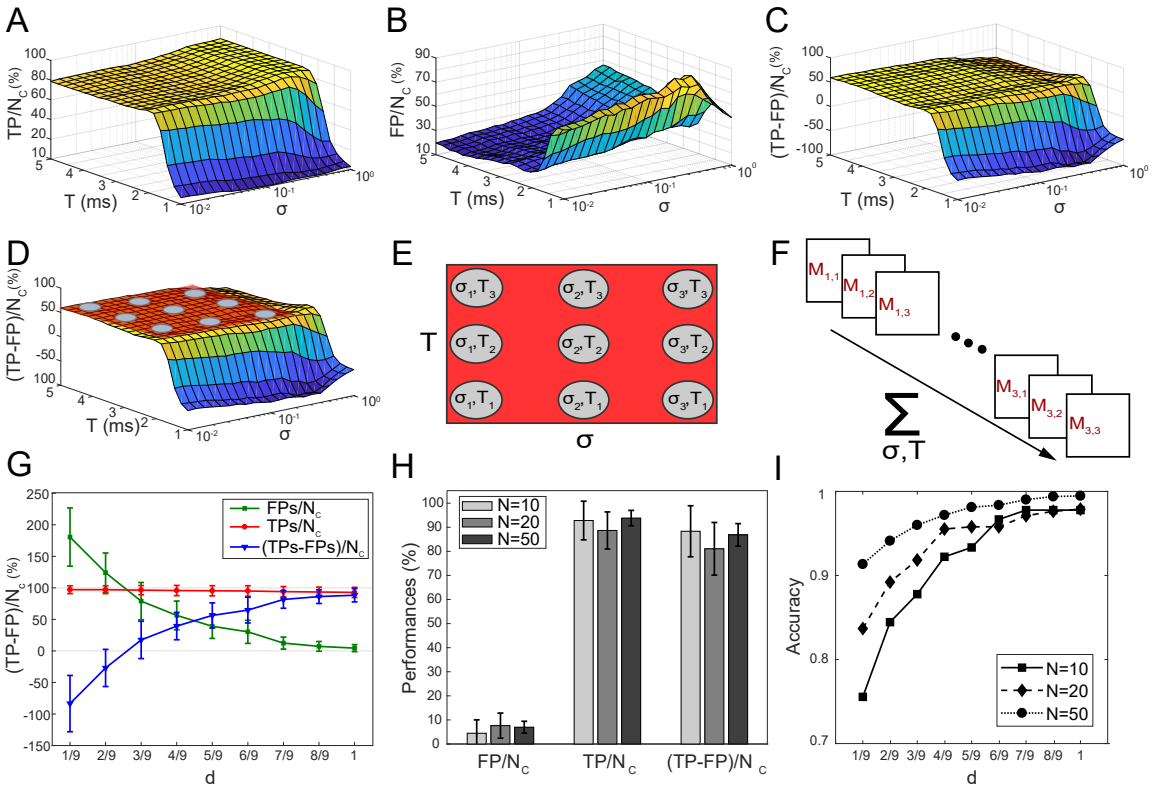

Figure 4: **Connectivity reconstruction and performance evaluation.** (A-C) Evaluation of the performance of the connectivity method under varying time window $(-T, +T)$, standard deviation σ, and for a fixed $\epsilon = 0.7$ ms, for one simulated network of 10 neurons. (A) Net number of detected true positives TP/N_c. (B) Net number of false positives FP/N_c. (C) Ratio $\Delta = (TP - FP)/N_c$ as chosen metric for evaluation. N_c is the known total number of connections in the simulated network. (D) Visual highlight on the behavior of Δ: a peak of performance is reached around 65%; low variability is proven for a wide range of T and σ (plateau indicated by the red plane). (E) Definition of a collection of $K = 9$ points p in the T-σ space for which the algorithm shows performances falling in correspondence of the plateau area. (F) Abstract representation of the statistical method for recognition of false positives connections and connectivity reconstruction. For each point a connectivity matrix M_p is computed, resulting in the computation of $K = 9$ different connectivity matrices for the same input network. Combination of the results enables computation of the frequency f_{jk} for each connection following Eq. (8). (G) Average (N=20) performances computed at different discrimination threshold d. The TPs remain roughly constant. On the other hand, the FPs decrease and fluctuate around very small percentage. The algorithm filters out the FPs that fluctuate at high frequency reaching best performances (85%) at $d = 1$. (H) Analysis of scaling properties. An average (N=20) number of TP/N_c, FP/N_c, and Δ was computed for 20 randomly generated networks with 10, 20, and 50 neurons, respectively. Very good performances are maintained constant for increasing network size. (G) Accuracy ACC indicator computed for different network sizes as a function of the discrimination threshold d. The error bars stand for the standard deviation of a dataset of 20 different networks.

defined the new indicator $\Delta = (TP - FP)/N_c$ which generally applies to all types of networks having different sizes and connectivities and, in computing the difference $TP - FP$, it highlights the method capabilities in rejecting or not the false positive connections.

First, we used TP/N_c, FP/N_c and Δ to investigate the effect of T, σ and ϵ (Figure 4A-C): from pre-selected ranges of these parameters based on observations on the simulated activity (see Section 2.4), we tuned T, σ and ϵ by looking at the method's performance in selected ranges ($T \in$ (1,5) ms, $\epsilon = 0.7$ ms and $\sigma \in (10^{-2}, 10^{0})$ ms). Most of the performance data Δ distributed to form a plateau in the T and σ space (Figure 4D). In this plateau region, we defined Q=9 points corresponding to the combinations $C_{\sigma,T} = (\sigma, T)$, with T =2.25 ms, 3.5 ms, 4.5 ms, and σ =0.013 ms, 0.1 ms, 0.63 ms and we used them to reconstruct the connectivity matrix based on the threshold frequency f_{jk} as formally described in Section 2.4.

The network model we adopted was used to generate spiking data useful to test and develop the connectivity algorithm based on analysis of correlations. However, this model was not intended to be representative of real biological neurons and does not reproduce all the specific features of electrical recordings from *in vitro* neuronal cultures. As a result, the range of parameters selected for the simulated case did not necessarily match the one for the real case and was later adapted to the data of recorded *in vitro* neuronal networks (see Section 4.2). However, the same parameters showed very high reproducibility in repeated experiments both with simulated networks and iPSC-derived neuronal systems. Scaling performances will be discussed later in the manuscript; however, T, σ and ϵ were not affected by the network size.

To validate the inference method and test its performance and scaling properties we used data generated via simulations of network models having varying size of 10, 20, and 50 nodes. For each network size, 20 different networks were randomly generated, simulated and then analyzed for connectivity reconstruction. For each tested network we compared the adjacency matrix reconstructed for a frequency f_{jk} (see Section 2.4) to the input connectivity matrix of the simulated model and computed the true positives (TP/N_c), false positives (FP/N_c) and confidence Δ (Figure 4G-H). For comparisons with the literature, we also calculated the Accuracy $ACC = (TP + TN)/N_{tot}$ of the investigated network model (Figure 4I).

3.2. Electrophysiological characterization of hiPSC-derived networks

Methods for generating cortical neurons from hiPSC, analyzing the composition of the resulting cell population, and culturing on MEA are described in Appendix B and C. hiPSC-derived cortical neurons plated on 48-wells format MEA plates were recorded every week. Recordings were acquired with the Maestro recording system and Axion Integrated Studio (Axion Biosystems). A butterworth band-pass (10-2500Hz) filter and adaptive threshold spike detector set to 5.5X standard deviations were applied to the raw data. Raster plots of neuronal spiking activity were generated using Axion Neural Metrics Tool, and the data were analyzed using Excel (Microsoft) and GraphPad Prism version 7.00 (GraphPad Software).

We used routines implemented in Matlab to analyze the electrophysiological recordings and identify the active neurons in the plate (Figure S.5 and Figure S.6). Figures 5A shows an example of network activity estimated through spike sorting techniques. We used principal component analysis (PCA) to extract similar features in the spikes' dataset to be used for clustering. We then grouped spikes with similar features into clusters, corresponding to different neurons. We used a k-means clustering approach consisting of partitioning n observations into k clusters in which each observation belonged to the cluster with the nearest mean. The clustering algorithm started with a pre-defined $k = 2$. This value was then automatically updated to the best k estimate based on observations

on the explained variance in PCA. The clustering was repeated 20 times using new initial cluster centroid positions (no change was observed for more than 20 replicates). The final output was the solution with lowest within-cluster sums of point-to-centroid distances. This approach did not always lead to an exact result. For critical cases, a visual test was performed to identify outliers among the individual waveforms from the same electrode and compared to the results of the AxIS software (*Axion Biosystem*).

3.3. Connectivity analysis in hiPSC-derived cultures

We used our algorithm to estimate the connectivity in recorded iPSC-derived neuronal networks at week 1, 2, 3, and 4 (Figure 5). We selected a range for the parameter T based on considerations of the mean propagation delays between synaptically connected neurons. While physiologically many variables contributes to neuronal delays, a rough indication of the delay in synaptically connected cortical neurons was estimated to be 6 - 14 ms [57]. We estimated similar conduction velocities and latency values in a previous study performed on basket and pyramidal neurons from the rat neocortex [58]. Given that monolayer networks of human iPSC-derived neurons may have temporal properties that differ from those observed in intact brain networks, we decided to avoid neglecting correlations that could negatively bias the inference performance (see Section 2.4) by considering a larger temporal window $(-22, 22)$ ms. The reconstruction analysis was then performed with $T \in 15, 22$ ms to include the propagation delays measured in cortical neurons (6 - 14 ms) and over-estimated values to limit over-filtering. For σ, observations on the recordings and the level of smoothing required for high-frequency noise removal led us to select $\sigma \in (0.3, 0.8)$ ms. We considered a fixed value of 3 ms equal to the average width of the correlation peaks (see Section 2.4). Within this range of parameters, we then selected $Q = 9$ points corresponding to the combinations $C_{\sigma,T} = (\sigma, T)$, with T =20 ms, 17.5 ms, 16 ms, and σ =0.4 ms, 0.55 ms, 0.7 ms.

We used a graph-based connectivity analysis to estimate developing connections between neurons. A common graph theory approach to measure the level of connectivity in a network is to investigate its centrality, which can be described as the capacity of a node to influence, or be influenced by, other system elements by virtue of its connection topology [59]. The simplest and most commonly used measure of centrality is node degree, which is the number of connections attached to a node. We calculated the average in-degree and out-degree of the vertexes of each directed graph corresponding to a reconstructed network by calculating all incoming and outgoing connections for each network vertex and then averaging over the total number of vertexes per network. The statistics was then extended to 20 different wells. A node scoring highly on a given centrality measure can be considered a hub. Here, we quantified the number of network hubs at each time point (from 1^{st} to 4^{th} week) by computing the centrality of the graph and ranking the vertexes based on the number of incoming connections. The most important vertexes were defined network hubs. We averaged this number over 20 reconstructed networks. Finally, we studied the integration and segregation properties of the networks [60] by computing the average Mean Path Length and Mean Cluster Coefficient (CCo). We calculated the Mean Path Length as the shortest path distance of all vertex pairs. Infinite (absent) connections between neurons were not considered in the calculation. With the use of Matlab routines, we also computed the CCo as the fraction of triangles around a node, which is equivalent to the fraction of node's neighbors that are neighbors of each other [61].

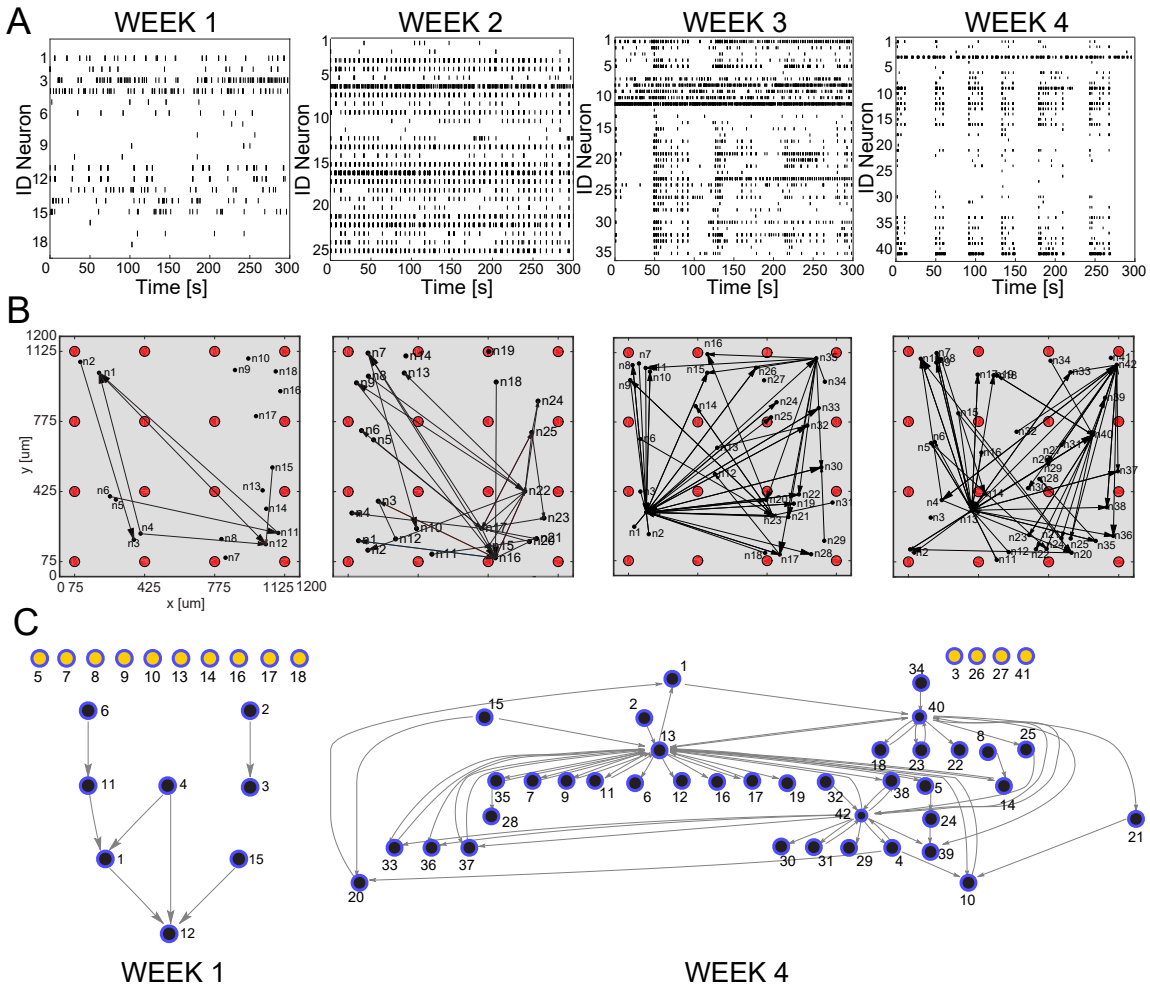

Figure 5: **Connectivity reconstruction from neural recordings of developing hiPSC-derived neurons** (A) Raster plots of the same MEA well at different time points during development: week 1, 2, 3, and 4 after plating. The four panels shows spiking signals from individual neurons (rows) obtained through spike sorting, PCA and k-means clustering of 300 sec recordings. The culture develops complex network features: from weakly active and randomly organized (individual spiking events), to very active and fully organized (network bursts). (B) Estimated effective connectivity of the developing culture whose activity is described in panel A. Each visual map consists of a 1.2 x 1.2 mm MEA plate (gray area), a 4-by-4 array of micro-electrodes (red circles) and the estimated directed connections (black arrows). The active neurons are represented by black dots; they are randomly distributed around their corresponding sensing electrode within a radius of 50 μm. (C) Directed graph relative to the culture at week 1 and week 4. The connectivity is equivalent to the one visualized in B but, for clarity and consistency with the main text, links between neurons are directed edges (arrows), active neurons are network nodes (blue: connected; yellow: independent). Given a MEA well and a specific time point, indexes refer to active neurons with recorded activity reported in (A). Note, neurons mapped at week 1 do not correspond to neurons mapped in the following weeks, although they are indicated with the same indexes.

4. Results

4.1. Numerical results

Figure 4A-C describes how the performances vary as function of $T \in$ (1,5) ms and the standard deviation $\sigma \in (10^{-2},10^{0})$ ms, for a fixed $\epsilon = 0.7$ ms equal to the width of the correlation peaks in the simulated data. The evaluation of the minimized G'_p enabled identification of 80-95% of the total positive direct connections present in the model (TP/N_c) in a wide range of $p = (\sigma, T)$, as demonstrated by the curve plateau in Figure 4A. The remaining percentage of connections corresponded to the net number of false connections (FP/N_c) that the algorithm was unable to sort out (Figure 4B) which remains very small for most parameter values. For small T ($T < 2$ ms), we observed a decay in sensitivity clearly due to over-filtering of true direct correlations. When doing so, the false positives first increased due to complete failure of the algorithm in recognizing connections in the small temporal range of observation and then rapidly decayed for very small T because no peaks could be found. This demonstrates the importance of choosing larger values both for T and for σ rather than smaller ones in order to avoid missing any correlation information that could negatively bias the algorithm performances. Figure 4C shows the resulting variation of Δ which reached a peak of confidence at 65% and was maintained constant for a wide range of parameters.

In Figure 4G we show averaged (N=20 networks) TP/N_c, FP/N_c and Δ as a function of the discrimination threshold d (Eq. 8). We note that, at a high discrimination threshold, while TP/N_c remained roughly constant (the same true positives were always detected, for all points), FP/N_c decreased towards very small percentages, smaller than the percentage corresponding to any of the p points. This is not surprising because the TP connections, which in most cases point to the interactions between the same pairs of neurons, were always observed for all points ($f_{jk} \approx 1$, f_{jk} is the frequency for each connection in the connectivity matrix - see Eq. 8). On the other hand, the false positives are just fluctuations of the algorithm as new false positive connections pointing every time to a different pair of neurons were constantly generated by the algorithm for all points p. As a result, the same false positive connections observed for a given pair of neurons are very unlikely detected by many different points, and at high frequency they are filtered out.
For example, for two given points p_1 and p_2 the algorithm detected 15% and 20% FPs, respectively; however, most of the FPs detected by point p_1 did not correspond to the ones detected by point p_2. On the other hand, the same two points p_1 and p_2 detected the same TPs. Through filtering, the TPs detected by both points are preserved, all FPs are discarded, resulting in 2% of FPs remaining, a percentage that is smaller than any percentage associated with each of the points. Importantly, this result demonstrates empirically our mathematical framework and it highlights its robustness in this example application.

Δ data showed average performances of 88.3%, 88.7%, and 86.8% for varying network sizes of 10, 20 and 50 neurons, respectively, therefore demonstrating a very reliable detection of connections and exceptional scaling properties in this example (Figure 4H).

For the sake of comparison with the literature, we show how the accuracy [56], averaged over 20 test networks with $N = 10$, 20, 50, respectively, changes with a selected frequency $f_{j,k}$. In Figure 4I, we observe that when the standard accuracy criteria ACC was used, the analysis quality largely improved with a maximum reached for f_{jk} =1. It is interesting to observe how the accuracy data for d =1/9, i.e. prior to using the reconstruction algorithm based on the discriminator threshold d (Figure 4I, d=1/9), showed performances already higher than 75% for a network of 10 neurons, and even higher for larger sizes, thus exceeding the ones obtained before standard thresholding in published connectivity methods [62]. The complete reconstruction algorithm led to a computational

accuracy close to 100% for all network sizes due to the further statistical pruning of false positive connections (Figure 4I, d =1).

It is worth noting that, compared to more conventional indicators, Δ is independent of the network's connectivity. Since we made the hypothesis that each node in the network model has the same average connectivity (preserved in- and out-degree) which does not increase with the network's size, we do not expect and we are not interested in seeing connectivity dependent variations. On the contrary, other metrics, such as the Receiving Operating Curve (ROC) or the Accuracy [56], largely change with the size and the connectivity properties of the network. For comparisons, we calculated the Accuracy $ACC = (TP + TN)/N_{tot}$ of the investigated network model. Because the definition of this measure is based on the hypothesis that larger networks feature higher connectivity, our data overestimate the performances, especially for high network sizes.

4.2. Measures of developing iPSC neural networks in vitro

We tested our connectivity algorithm on networks of human iPSC-derived neurons cultured on 48-well MEA plates (*Axion Biosystem*). The activity was recorded periodically over four weeks (Figure S.3) to investigate network development. In parallel, immunofluorescent analyses (Figure S.4) of the composition of the neuronal population showed a mix of excitatory and inhibitory neurons, as well as astrocytes, resembling the physiological composition of an *in-vivo* neural network.

The data show an increase in the level of activity as a function of the developmental phase, as well as the appearance of repetitive firing patterns and the formation of well-organized network bursts. Analysis of activity parameters, bursting patterns and emergence of network bursting are presented in Figure S.3.

We used our algorithm to estimate the connectivity in the recorded iPSC-derived neural networks at week 1, 2, 3, and 4 (Figure 5B). Based on the position of each electrode, we estimated the localization of the recorded neurons. The neurons have been randomly distributed around their corresponding recording electrode, within a radius of 50 μm, as this is the expected sensitivity range of MEA electrodes. Figure 5C reports the corresponding graph-based schema of the reconstructed adjacency matrices in B, for week 1 and 4, respectively. Both descriptions clearly demonstrate maturation of the network and increase in overall connectivity, as well as the formation of a few highly connected sub-networks within the culture.

To generate a more quantitative estimation of these network features, we used a graph-theory based analysis (Figure 6). The larger number of active neurons and detected links in most developed networks is in accordance with the increasing levels of activity of the culture at later time points (Figure 6A). We observed that during spontaneous activity, the in- and out-degrees for different neurons were almost equally distributed among the active neurons, and showed an increasing trend as a function of the culture's age. Moreover, we observed formation of a specific network topology characterized by a connectivity highly centralized around a few super-hubs reciprocally linked to neighboring cells (large average degree), and a few remaining, poorly connected neurons (small average degree) (Figure 6B). These data confirm what is visually described in the connectivity maps and correlate with the network burst activity in the way the connectivity topology changes from random and unorganized, with most of the neurons isolated and poorly connected, to extremely structured and centered around a few hubs, a topology that becomes more evident with maturation. We also studied the integration and segregation properties of cultured human iPSC-derived neural

networks (6C). The Mean Path Length is fairly constant and does not change for increasing numbers of new connections. On the other hand, the Mean Cluster Coefficient (CCo) is low and decreases with the level of maturation of the network. This feature is indicative of more favored segregation versus integration, with formation of highly integrated network units (hubs), similarly to observations reported by Livesey and colleagues [14] using rabies-virus-based trans-synaptic tracings of hiPSC-derived neuronal networks.

Discussion

In this work, we demonstrated a new model-free based approach to reconstruct effective and functional connections from *in vitro* neuronal networks recorded on MEAs. Our algorithm offers several fundamental differences resulting in critical advancements compared to the state-of-the-art connectivity techniques, including correlation and transfer entropy variants [25, 62]. To the best of our knowledge, model-free connectivity inference techniques are not able to reconstruct the effective - causal and direct - connections of a recorded neuronal network because they are either missing the causality of signaling or include confounding apparent connections (common input or common output) and multi-neuron pathways. Here, we defined a fundamental mathematical rule that decomposes the misleading temporal information contained in the network's temporal correlations into a set of direct, causal dependencies between the circuit's neurons via selective identification and elimination of false positive connections (Figure 2).

Our method does not require any post-inference thresholding and it only depends on three fundamental parameters - T, σ and ϵ - which can be easily obtained as explained in the text, and whose choice will be automated in future software release.

Evaluation of the performances on synthetic data from simulated random networks of neurons demonstrated a number of critical improvements compared to published algorithms by showing inference of causal, uni- and bi-directional connectivity directly from MEA data with a computational accuracy close to 1 and an excellent rate of rejection of false positive connections (Figure 4).

In terms of scalability, our algorithm matches the scalability properties of most of the state-of-the-art connectivity methods which, being based on pairwise statistical and correlation studies, scale with a complexity of the order of $O(n^2)$. On the other hand, techniques such as partial correlation, matrix deconvolution or deep learning, which we found to be the only approaches able to distinguish between apparent and direct connectivity (see Figure 1), have high computational complexity. For example, partial correlation yields a complexity of $O(n^3)$.

Importantly, in this work we did not attempt to simulate and analyze large artificial neural networks where the number of nodes and connections aim to mimic the massive synaptic connections present in the brain. We simulated sparse networks instead, having connectivity $N_c < N_{tot}$, and hypothesized average constant connectivity for larger network sizes. This simplified model was quite accurate in describing *in vitro* networks of biological neurons like the cultures of iPSC-derived neurons we investigated (see Figure S.4). Larger networks can be simulated and tested at higher computational expenses. Based on observations on the algorithm performances, we expect approximately constant performances for increasing number of neural nodes; on the other hand, we can only speculate on the inference properties in highly connected networks ($N_c \sim N_{tot}$) because of increased difficulties in properly modeling their simulated activity, as well as the anticipated increases in computational power required for processing these analyses. We expect decaying performance for

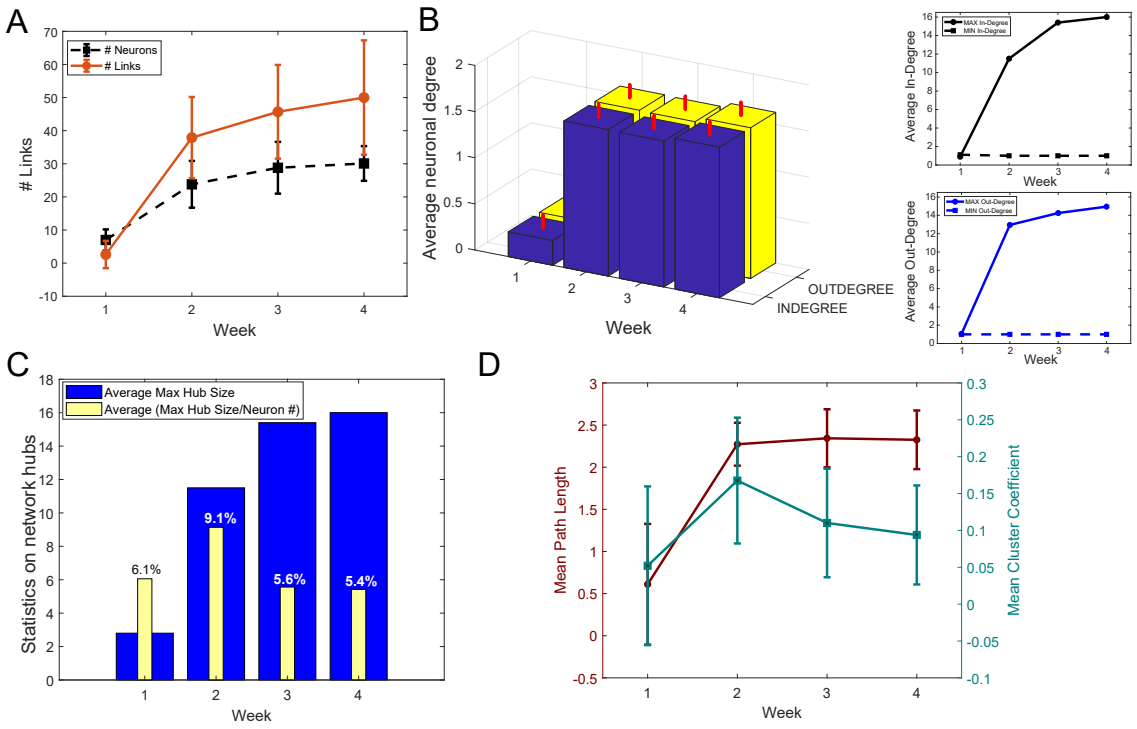

Figure 6: **Graph-theory based analysis of network connectivity in developing hiPSC-derived neuronal-network** (A) Average number (N=20) of active neurons (black) and detected connections (red) in MEA wells recorded at week 1, 2, 3, and 4 after plating. The error bars represent the standard deviations for a dataset of 20 different MEA wells. (B) (Left panel) Statistics (N=20) on the neuronal in- (number of input connections) (blue) and out-degree (number of output connections) (yellow). The vertical red bars stand for the standard deviations of in- and out-degree data. (Right panel) Average maximum (continuous line) and minimum (dashed line) in- (top) and out- (bottom) degree. The number of in- and out- degree is equally distributed with equivalent raising behavior as a function of the cultures' developmental stage. (C) Statistics on network hubs as a function of the culture's age. In blue, average (N=20) maximum hub size. We used the in-degree centrality measures for hub detection and characterization. In yellow, percentage of neurons that function as network hubs relative to the total number of active neurons in the well (value averaged over 20 wells). More mature networks include few super-hubs (∼5% of the total number of neurons) with increase in size as demonstrated by the raising number of incoming connections at week 3 and 4. (D) Characterization of network segregation and integration properties. Values in the graph correspond to the mean Path Length (PL) and mean Clustering Coefficient (CCo) calculated for each well at week 1, 2 ,3, and 4 after plating and then averaged over 20 wells. The error bars correspond to the standard deviation of 20 different measures. The mean PL corresponds to the average shortest path length in the networks. Infinite (absent) connections between neurons were not considered in its calculation. The PL is very low for highly immature cultures where only sparse activity from individual neurons was mainly registered. It increases as soon as connections are formed (week 2) but no longer changes with the number of new connections (week 2, 3, 4). The CCo is low and decreases with the maturation of the network as indication of favored segregation versus integration with increasing number of independent but highly-integrated network units (hubs).

networks of very high complexity due to many overlapping correlation effects from multiple cells, a problem that will require further investigation and will be addressed in future studies.

As a direct example, we have used the spontaneous firing of cultured networks of iPSC-derived neurons to reconstruct the corresponding connectivity maps as a function of the network developmental stage (Figure 6). The estimated connectivity (Figure 5) combined with quantitative analyses, such as graph-theory approaches (Figure 6), enabled us to describe the developmental progress of the cultures, thus demonstrating the capability of detecting basic neuronal features such as the increased synaptic connectivity and the formation of few, highly connected network hubs. These latter are both indexes of more mature neuronal circuits and agree well with higher spiking frequencies and network burst generation observed in mature neuronal cultures [63].

Further work must also be done to extend this approach to the explicit identification of inhibitory inputs and their role. We note that inhibitory connections are implicitly defined in the reconstructed network; however, in contrast to more recent works [64], our analysis has not explicitly distinguished them from excitatory links. We have estimated the connectivity matrix of a sub-network which includes the strongest recurrent links in the neuronal culture, major determinants of spontaneous activity [65] that we are interested in perturbing and analyzing.

Importantly, spatio-temporal information is implicitly contained in the estimated connectivity and delay map too; we expect therefore that, when used in combination with novel computational methodologies [66, 58, 67], our method will help reveal more fundamental network properties crucial to the understanding of the relationships between network topology, dynamic signaling and network functions in healthy and disease models.

5. Conclusions

We have presented an innovative approach to map the effective connectivity of neural networks from multi-electrode array data. The tool that we have developed offers critical improvements over available methods for estimating functional connectivity. Notably, our connectivity algorithm succeeds in detecting direct connections between neurons through a mathematically rigorous selection scheme that distinguishes between apparent or non-direct links and direct ones, therefore enabling identification of directed causal relationships between connected neurons. In addition, it has good scaling capabilities and can be further extended, optimized, and possibly integrated with already in-use techniques. Furthermore, it will be broadly applicable to experimental techniques for neural activation and recording, increasing its utility for the analyses of spontaneous neural activity patterns, as well as neuronal responses to pharmacological perturbations and electrical and optogenetic stimulations [68, 69, 70, 71, 72].

Acknowledgments

The authors thank Fabio L. Traversa for fruitful and constructive discussions. This work was funded by a Swiss National Science Foundation (SNSF) Mobility Fellowship (P2ELP2_168553) to FP, a NIMH U19MH106434 to AB, and in part by unrestricted funds to the Center for Engineered Natural Intelligence (CENI).

Author contributions

F.P. conceived the original hypothesis and theoretical approach, with additional contributions by G.S.. F.P., D.P., A.B. and G.S. conceived the project. F.P. developed and implemented the theory, organized the study and carried out all the computational analyses. D.P. and A.B. designed and organized the experimental studies. D.P. carried out all experiments and related analyses. All authors have contributed in interpreting the results and writing the manuscript.

Competing financial interests

The authors declare no competing financial interests.

Materials and correspondence

Correspondence and request for materials should be addressed to G.S. (gsilva@ucsd.edu) and A.B (abang@sbpdiscovery.org).

References

[1] M. Chiappalone, A. Vato, L. Berdondini, M. Koudelka-Hep, S. Martinoia, Networks dynamics and synchronous activity in cultured cortical neurons, International Journal of Neural Systems 17 (02) (2007) 87–103. doi:10.1142/s0129065707000968.

[2] D. Wagenaar, J. Pine, S. Potter, An extremely rich repertoire of bursting patterns during the development of cortical cultures, BMC Neuroscience 7 (1) (2006) 11. doi:10.1186/1471-2202-7-11.

[3] R. Segev, Y. Shapira, M. Benveniste, E. Ben-Jacob, Observations and modeling of synchronized bursting in two-dimensional neural networks, Physical Review E 64 (1) (Jun. 2001). doi:10.1103/physreve.64.011920.

[4] M. Meister, R. Wong, D. Baylor, C. Shatz, Synchronous bursts of action potentials in ganglion cells of the developing mammalian retina, Science 252 (5008) (1991) 939–943. doi:10.1126/science.2035024.

[5] M. J. Gutnick, B. W. Connors, D. A. Prince, Mechanisms of neocortical epileptogenesis in vitro, Journal of Neurophysiology 48 (6) (1982) 1321–1335. doi:10.1152/jn.1982.48.6.1321.

[6] J. Eckmann, O. Feinerman, L. Gruendlinger, E. Moses, J. Soriano, T. Tlusty, The physics of living neural networks, Physics Reports 449 (1-3) (2007) 54–76. doi:10.1016/j.physrep.2007.02.014.

[7] R. Yuste, From the neuron doctrine to neural networks, Nature Reviews Neuroscience 16 (8) (2015) 487–497. doi:10.1038/nrn3962.

[8] S. Marom, G. Shahaf, Development, learning and memory in large random networks of cortical neurons: lessons beyond anatomy, Quarterly Reviews of Biophysics 35 (01) (feb 2002). doi:10.1017/s0033583501003742.

[9] T. Opitz, A. D. D. Lima, T. Voigt, Spontaneous development of synchronous oscillatory activity during maturation of cortical networks in vitro, Journal of Neurophysiology 88 (5) (2002) 2196–2206. doi:10.1152/jn.00316.2002.

[10] P. S. Churchland, T. J. Sejnowski, The Computational Brain, MIT Press, 1992.

[11] O. Sporns, G. Tononi, R. Kötter, The human connectome: A structural description of the human brain, PLoS Computational Biology 1 (4) (2005) e42. doi:10.1371/journal.pcbi.0010042.

[12] K. Takahashi, K. Tanabe, M. Ohnuki, M. Narita, T. Ichisaka, K. Tomoda, S. Yamanaka, Induction of pluripotent stem cells from adult human fibroblasts by defined factors, Cell 131 (5) (2007) 861–872. doi:10.1016/j.cell.2007.11.019.

[13] J. Yu, M. A. Vodyanik, K. Smuga-Otto, J. Antosiewicz-Bourget, J. L. Frane, S. Tian, J. Nie, G. A. Jonsdottir, V. Ruotti, R. Stewart, I. I. Slukvin, J. A. Thomson, Induced pluripotent stem cell lines derived from human somatic cells, Science 318 (5858) (2007) 1917–1920. doi:10.1126/science.1151526.

[14] P. Kirwan, B. Turner-Bridger, M. Peter, A. Momoh, D. Arambepola, H. P. C. Robinson, F. J. Livesey, Development and function of human cerebral cortex neural networks from pluripotent stem cells in vitro, Development 142 (18) (2015) 3178–3187. doi:10.1242/dev.123851.

[15] A. Odawara, Y. Saitoh, A. Alhebshi, M. Gotoh, I. Suzuki, Long-term electrophysiological activity and pharmacological response of a human induced pluripotent stem cell-derived neuron and astrocyte co-culture, Biochemical and Biophysical Research Communications 443 (4) (2014) 1176–1181. doi:10.1016/j.bbrc.2013.12.142.

[16] A. Sarkar, A. Mei, A. C. Paquola, S. Stern, C. Bardy, J. R. Klug, S. Kim, N. Neshat, H. J. Kim, M. Ku, M. N. Shokhirev, D. H. Adamowicz, M. C. Marchetto, R. Jappelli, J. A. Erwin, K. Padmanabhan, M. Shtrahman, X. Jin, F. H. Gage, Efficient generation of CA3 neurons from human pluripotent stem cells enables modeling of hippocampal connectivity in vitro, Cell Stem Cell 22 (5) (2018) 684–697.e9. doi:10.1016/j.stem.2018.04.009.

[17] K. J. Brennand, A. Simone, J. Jou, C. Gelboin-Burkhart, N. Tran, S. Sangar, Y. Li, Y. Mu, G. Chen, D. Yu, S. McCarthy, J. Sebat, F. H. Gage, Modelling schizophrenia using human induced pluripotent stem cells, Nature 473 (7346) (2011) 221–225. doi:10.1038/nature09915.

[18] B. J. Wainger, E. Kiskinis, C. Mellin, O. Wiskow, S. S. Han, J. Sandoe, N. P. Perez, L. A. Williams, S. Lee, G. Boulting, J. D. Berry, R. H. Brown, M. E. Cudkowicz, B. P. Bean, K. Eggan, C. J. Woolf, Intrinsic membrane hyperexcitability of amyotrophic lateral sclerosis patient-derived motor neurons, Cell Reports 7 (1) (2014) 1–11. doi:10.1016/j.celrep.2014.03.019.

[19] C. M. Woodard, B. A. Campos, S.-H. Kuo, M. J. Nirenberg, M. W. Nestor, M. Zimmer, E. V. Mosharov, D. Sulzer, H. Zhou, D. Paull, L. Clark, E. E. Schadt, S. P. Sardi, L. Rubin, K. Eggan, M. Brock, S. Lipnick, M. Rao, S. Chang, A. Li, S. A. Noggle, iPSC-derived dopamine neurons reveal differences between monozygotic twins discordant for parkinson's disease, Cell Reports 9 (4) (2014) 1173–1182. doi:10.1016/j.celrep.2014.10.023.

[20] I. Canals, J. Soriano, J. G. Orlandi, R. Torrent, Y. Richaud-Patin, S. Jiménez-Delgado, S. Merlin, A. Follenzi, A. Consiglio, L. Vilageliu, D. Grinberg, A. Raya, Activity and high-order effective connectivity alterations in sanfilippo c patient-specific neuronal networks, Stem Cell Reports 5 (4) (2015) 546–557. doi:10.1016/j.stemcr.2015.08.016.

[21] S. Nageshappa, C. Carromeu, C. A. Trujillo, P. Mesci, I. Espuny-Camacho, E. Pasciuto, P. Vanderhaeghen, C. M. Verfaillie, S. Raitano, A. Kumar, C. M. B. Carvalho, C. Bagni, M. B. Ramocki, B. H. S. Araujo, L. B. Torres, J. R. Lupski, H. V. Esch, A. R. Muotri, Altered neuronal network and rescue in a human MECP2 duplication model, Molecular Psychiatry 21 (2) (2015) 178–188. doi:10.1038/mp.2015.128.

[22] C. A. Trujillo, P. D. Negraes, B. Hrvoj-Mihic, M. F. Lins, K. Semendeferi, A. R. Muotri, Brain in a dish, in: Genomics, Circuits, and Pathways in Clinical Neuropsychiatry, Elsevier, 2016, pp. 117–132. doi:10.1016/b978-0-12-800105-9.00008-1.

[23] J. J. Fink, E. S. Levine, Uncovering true cellular phenotypes: Using induced pluripotent stem cell-derived neurons to study early insults in neurodevelopmental disorders, Frontiers in Neurology 9 (apr 2018). doi:10.3389/fneur.2018.00237.

[24] M. C. Silva, S. J. Haggarty, Human pluripotent stem cell–derived models and drug screening in CNS precision medicine, Annals of the New York Academy of Sciences (mar 2019). doi:10.1111/nyas.14012.

[25] I. M. de Abril, J. Yoshimoto, K. Doya, Connectivity inference from neural recording data: Challenges, mathematical bases and research directions, Neural Networks 102 (2018) 120–137. doi:10.1016/j.neunet.2018.02.016.

[26] H. E. Wang, C. G. Bénar, P. P. Quilichini, K. J. Friston, V. K. Jirsa, C. Bernard, A systematic framework for functional connectivity measures, Frontiers in Neuroscience 8 (dec 2014). doi:10.3389/fnins.2014.00405.

[27] O. Sporns, Structure and function of complex brain networks., Dialogues in clinical neuroscience 15 (2013) 247–262.

[28] V. A. Makarov, F. Panetsos, O. de Feo, A method for determining neural connectivity and inferring the underlying network dynamics using extracellular spike recordings, Journal of Neuroscience Methods 144 (2) (2005) 265–279. doi:10.1016/j.jneumeth.2004.11.013.

[29] K. Friston, L. Harrison, W. Penny, Dynamic causal modelling, NeuroImage 19 (4) (2003) 1273–1302. doi:10.1016/s1053-8119(03)00202-7.

[30] A. R. McLntosh, F. Gonzalez-Lima, Structural equation modeling and its application to network analysis in functional brain imaging, Human Brain Mapping 2 (1-2) (1994) 2–22. doi:10.1002/hbm.460020104.

[31] M. Garofalo, T. Nieus, P. Massobrio, S. Martinoia, Evaluation of the performance of information theory-based methods and cross-correlation to estimate the functional connectivity in cortical networks, PLoS ONE 4 (8) (2009) e6482. doi:10.1371/journal.pone.0006482.

[32] E. Pereda, R. Q. Quiroga, J. Bhattacharya, Nonlinear multivariate analysis of neurophysiological signals, Progress in Neurobiology 77 (1-2) (2005) 1–37. doi:10.1016/j.pneurobio.2005.10.003.

[33] K. J. Friston, Functional and effective connectivity: A review, Brain Connectivity 1 (1) (2011) 13–36. doi:10.1089/brain.2011.0008.

[34] J. L. Rodgers, W. A. Nicewander, Thirteen Ways to Look at the Correlation Coefficient, The American Statistician 42 (1) (1988) 59. doi:10.2307/2685263.

[35] M. J. Hinich, C. S. Clay, The application of the discrete Fourier transform in the estimation of power spectra, coherence, and bispectra of geophysical data, Reviews of Geophysics 6 (3) (1968) 347. doi:10.1029/rg006i003p00347.

[36] A. Grinsted, J. C. Moore, S. Jevrejeva, Application of the cross wavelet transform and wavelet coherence to geophysical time series, Nonlinear Processes in Geophysics 11 (5/6) (2004) 561–566. doi:10.5194/npg-11-561-2004.

[37] F. L. da Silva, J. P. Pijn, P. Boeijinga, Interdependence of EEG signals: Linear vs. nonlinear Associations and the significance of time delays and phase shifts, Brain Topography 2 (1-2) (1989) 9–18. doi:10.1007/bf01128839.

[38] P. Grassberger, T. Schreiber, C. Schaffrath, NONLINEAR TIME SEQUENCE ANALYSIS, International Journal of Bifurcation and Chaos 01 (03) (1991) 521–547. doi:10.1142/s0218127491000403.

[39] R. Q. Quiroga, A. Kraskov, T. Kreuz, P. Grassberger, Performance of different synchronization measures in real data: A case study on electroencephalographic signals, Physical Review E 65 (4) (mar 2002). doi:10.1103/physreve.65.041903.

[40] A. M. Bastos, J.-M. Schoffelen, A tutorial review of functional connectivity analysis methods and their interpretational pitfalls, Frontiers in Systems Neuroscience 9 (jan 2016). doi:10.3389/fnsys.2015.00175.

[41] S. Ito, M. E. Hansen, R. Heiland, A. Lumsdaine, A. M. Litke, J. M. Beggs, Extending Transfer Entropy Improves Identification of Effective Connectivity in a Spiking Cortical Network Model, PLoS ONE 6 (11) (2011) e27431. doi:10.1371/journal.pone.0027431.

[42] L. A. Baccalá, K. Sameshima, Partial directed coherence: a new concept in neural structure determination, Biological Cybernetics 84 (6) (2001) 463–474. doi:10.1007/pl00007990.

[43] Y. Saito, H. Harashima, Tracking of information within multichannel EEG record—Causal analysis in EEG, in: N. Yamaguchi, K. Fujisawa (Eds.), Recent Advances in EEG and EMG data processing, Elsevier, Amsterdam, 1981, pp. 133–146.

[44] M. Lungarella, A. Pitti, Y. Kuniyoshi, Information transfer at multiple scales, Physical Review E 76 (5) (nov 2007). doi:10.1103/physreve.76.056117.

[45] C. W. J. Granger, Investigating Causal Relations by Econometric Models and Cross-spectral Methods, Econometrica 37 (3) (1969) 424. doi:10.2307/1912791.

[46] A. K. Seth, A MATLAB toolbox for Granger causal connectivity analysis, Journal of Neuroscience Methods 186 (2) (2010) 262–273. doi:10.1016/j.jneumeth.2009.11.020.

[47] A. Sutera, A. Joly, V. Franois-Lavet, Z. A. Qiu, G. Louppe, D. Ernst, P. Geurts, Simple Connectome Inference from Partial Correlation Statistics in Calcium Imaging, in: Neural Connectomics Challenge, Springer International Publishing, 2017, pp. 23–36. doi:10.1007/978-3-319-53070-3_2.

[48] J. Orlandi, B. Ray, D. Battaglia, I. Guyon, V. Lemaire, M. Saeed, A. Statnikov, O. Stetter, J. Soriano, First connectomics challenge: From imaging to connectivity, in: Neural Connectomics Challenge, Springer International Publishing, 2017, pp. 1–22. doi:10.1007/978-3-319-53070-3_1.

[49] I. M. de Abril, A. Nowé, Supervised neural network structure recovery, in: D. Battaglia, I. Guyon, V. Lemaire, J. Soriano (Eds.), Proceedings of the Neural Connectomics Workshop at ECML 2014, Vol. 46 of Proceedings of Machine Learning Research, PMLR, 2015, pp. 37–44. URL http://proceedings.mlr.press/v46/abril15.html

[50] L. Romaszko, Signal correlation prediction using convolutional neural networks, in: Neural Connectomics Challenge, Springer International Publishing, 2017, pp. 47–60. doi:10.1007/978-3-319-53070-3_4.

[51] S. Song, P. J. Sjöström, M. Reigl, S. Nelson, D. B. Chklovskii, Highly nonrandom features of synaptic connectivity in local cortical circuits, PLoS Biology 3 (3) (2005) e68. doi:10.1371/journal.pbio.0030068.

[52] A. Roxin, V. Hakim, N. Brunel, The statistics of repeating patterns of cortical activity can be reproduced by a model network of stochastic binary neurons, Journal of Neuroscience 28 (42) (2008) 10734–10745. doi:10.1523/jneurosci.1016-08.2008.

[53] R. Bracewell, Convolution Theorem, in: The Fourier Transform and Its Applications, 3rd ed., 1999.

[54] B. W. Silverman, Density Estimation for Statistics and Data Analysis, Chapman and Hall/CRC, 1986.

[55] E. Izhikevich, Simple model of spiking neurons, IEEE Transactions on Neural Networks 14 (6) (2003) 1569–1572. doi:10.1109/tnn.2003.820440.

[56] D. Poli, V. P. Pastore, S. Martinoia, P. Massobrio, From functional to structural connectivity using partial correlation in neuronal assemblies, Journal of Neural Engineering 13 (2) (2016) 026023. doi:10.1088/1741-2560/13/2/026023.

[57] G. Gonzalez-Burgos, Horizontal synaptic connections in monkey prefrontal cortex: An in vitro electrophysiological study, Cerebral Cortex 10 (1) (2000) 82–92. doi:10.1093/cercor/10.1.82.

[58] F. Puppo, V. George, G. A. Silva, An optimized structure-function design principle underlies efficient signaling dynamics in neurons, Scientific Reports 8 (1) (jul 2018). doi:10.1038/s41598-018-28527-2.

[59] S. Oldham, A. Fornito, The development of brain network hubs, Developmental Cognitive Neuroscience 36 (2019) 100607. doi:10.1016/j.dcn.2018.12.005.

[60] O. Sporns, Network attributes for segregation and integration in the human brain, Current Opinion in Neurobiology 23 (2) (2013) 162–171. doi:10.1016/j.conb.2012.11.015.

[61] M. E. J. Newman, The Structure and Function of Complex Networks, SIAM Review 45 (2) (2003) 167–256. doi:10.1137/s003614450342480.

[62] V. P. Pastore, D. Poli, A. Godjoski, S. Martinoia, P. Massobrio, ToolConnect: A functional connectivity toolbox for in vitro networks, Frontiers in Neuroinformatics 10 (mar 2016). doi:10.3389/fninf.2016.00013.

[63] C. A. Trujillo, R. Gao, P. D. Negraes, J. Gu, J. Buchanan, S. Preissl, A. Wang, W. Wu, G. G. Haddad, I. A. Chaim, A. Domissy, M. Vandenberghe, A. Devor, G. W. Yeo, B. Voytek, A. R. Muotri, Complex oscillatory waves emerging from cortical organoids model early human brain network development, Cell Stem Cell 25 (4) (2019) 558–569.e7. doi:10.1016/j.stem.2019.08.002.

[64] V. P. Pastore, P. Massobrio, A. Godjoski, S. Martinoia, Identification of excitatory-inhibitory links and network topology in large-scale neuronal assemblies from multi-electrode recordings, PLOS Computational Biology 14 (8) (2018) e1006381. doi:10.1371/journal.pcbi.1006381.

[65] O. Stetter, D. Battaglia, J. Soriano, T. Geisel, Model-free reconstruction of excitatory neuronal connectivity from calcium imaging signals, PLoS Computational Biology 8 (8) (2012) e1002653. doi:10.1371/journal.pcbi.1002653.

[66] G. A. Silva, The Effect of Signaling Latencies and Node Refractory States on the Dynamics of Networks, Neural Computation 31 (12) (2019) 2492–2522. doi:10.1162/neco_a_01241.

[67] J. M. L. Budd, K. Kovács, A. S. Ferecskó, P. Buzás, U. T. Eysel, Z. F. Kisvárday, Neocortical axon arbors trade-off material and conduction delay conservation, PLoS Computational Biology 6 (3) (2010) e1000711. doi:10.1371/journal.pcbi.1000711.

[68] M. Thunemann, Y. Lu, X. Liu, K. Kılıç, M. Desjardins, M. Vandenberghe, S. Sadegh, P. A. Saisan, Q. Cheng, K. L. Weldy, H. Lyu, S. Djurovic, O. A. Andreassen, A. M. Dale, A. Devor, D. Kuzum, Deep 2-photon imaging and artifact-free optogenetics through transparent graphene microelectrode arrays, Nature Communications 9 (1) (may 2018). doi:10.1038/s41467-018-04457-5.

[69] D. R. Hochbaum, Y. Zhao, S. L. Farhi, N. Klapoetke, C. A. Werley, V. Kapoor, P. Zou, J. M. Kralj, D. Maclaurin, N. Smedemark-Margulies, J. L. Saulnier, G. L. Boulting, C. Straub, Y. K. Cho, M. Melkonian, G. K.-S. Wong, D. J. Harrison, V. N. Murthy, B. L. Sabatini, E. S. Boyden, R. E. Campbell, A. E. Cohen, All-optical electrophysiology in mammalian neurons using engineered microbial rhodopsins, Nature Methods 11 (8) (2014) 825–833. doi:10.1038/nmeth.3000.

[70] J. Müller, M. Ballini, P. Livi, Y. Chen, M. Radivojevic, A. Shadmani, V. Viswam, I. L. Jones, M. Fiscella, R. Diggelmann, A. Stettler, U. Frey, D. J. Bakkum, A. Hierlemann, High-resolution CMOS MEA platform to study neurons at subcellular, cellular, and network levels, Lab on a Chip 15 (13) (2015) 2767–2780. doi:10.1039/c5lc00133a.

[71] C. Nguyen, H. Upadhyay, M. Murphy, G. Borja, E. J. Rozsahegyi, A. Barnett, T. Brookings, O. B. McManus, C. A. Werley, Simultaneous voltage and calcium imaging and optogenetic stimulation with high sensitivity and a wide field of view, Biomedical Optics Express 10 (2) (2019) 789. doi:10.1364/boe.10.000789.

[72] E. S. Boyden, F. Zhang, E. Bamberg, G. Nagel, K. Deisseroth, Millisecond-timescale, genetically targeted optical control of neural activity., Nature neuroscience 8 (2005) 1263–1268. doi:10.1038/nn1525.